The value of Seasonal Flow Forecasts for reservoir operations in enhancing drought management in South Korea (Supplementary materials)

S1. Pareto-front normalisation

Given the dimensional disparity between the two objectives (SSD, SVD), transforming the Pareto front can offer advantages, and normalisation is considered the most robust approach (Marler and Arora, 2004). Therefore, before applying each MCDM method, we normalized the Pareto-front. Among the numerous normalisation methods, we applied the widely used Min-max method. This method holds advantages in preserving the relationships among the original data (Han et al., 2012) and has demonstrated good performance, particularly in the SAW method (Mathew et al., 2017; Vafaei et al., 2022). Although this method is known for its sensitivity to outliers in extreme data (Han et al., 2012), the Pareto front generated from Eqs. 5 and 6 consists of continuous points without outliers. It performs a linear transformation on the original data and confines each objective in the range 0 to 1 as described by the following equation:

$$x_{normalised} = \frac{x - \min(x)}{\max(x) - \min(x)} \tag{S1}$$

where $x, \min(x)$ and $\max(x)$ represent a point, minimum and maximum point within the Pareto fronts, respectively.

S2. Multi-Criteria Decision-Making method

The SAW method, which is one of frequently employed methods in decision-making (Arsyah et al., 2021), ranks the alternatives based on their weighted sum performance (Fishburn, 1967). Given our aim to minimize SSD and SVD, the selected compromise solution is the one with the smallest weighted sum, as expressed below:

$$Compromise\ solution_{SAW} = \min(w_{SSD} \times SSD_i + w_{SVD} \times SVD_i) \tag{S2}$$

where, w_{SSD} and w_{SVD} are the weights for supply and storage. SSD_i and SVD_i represent the normalized objectives at the *i*th point within the Pareto front (*i* = 1, … ,100). In this study, we consider the 'balanced' method where equal weights are assigned to each objective ($w_{SSD} = w_{SVD} = 0.5$), as well as the 'storage-prioritized' and 'supply-prioritized' methods, which prioritize storage ($w_{SSD} = 0.4$, $w_{SVD} = 0.6$) and supply ($w_{SSD} = 0.6$, $w_{SVD} = 0.4$), respectively.

The 'variable weighting' method, which uses again Eq. S2 but assigns different weights according to the storage volume at the time when the decision is taken. We applied this method in two ways: the 'simple selective' method, which adopts the same weights as in the SAW methods but varying them depending on storage status, and the 'multi-weight' method, which applies more detailed procedure to allocate weights based on storage status. In doing so, we analysed around 20 years of historical storage records to divide the storage into multiple ranges, then specified a method or weight for each range (see Figure SI).

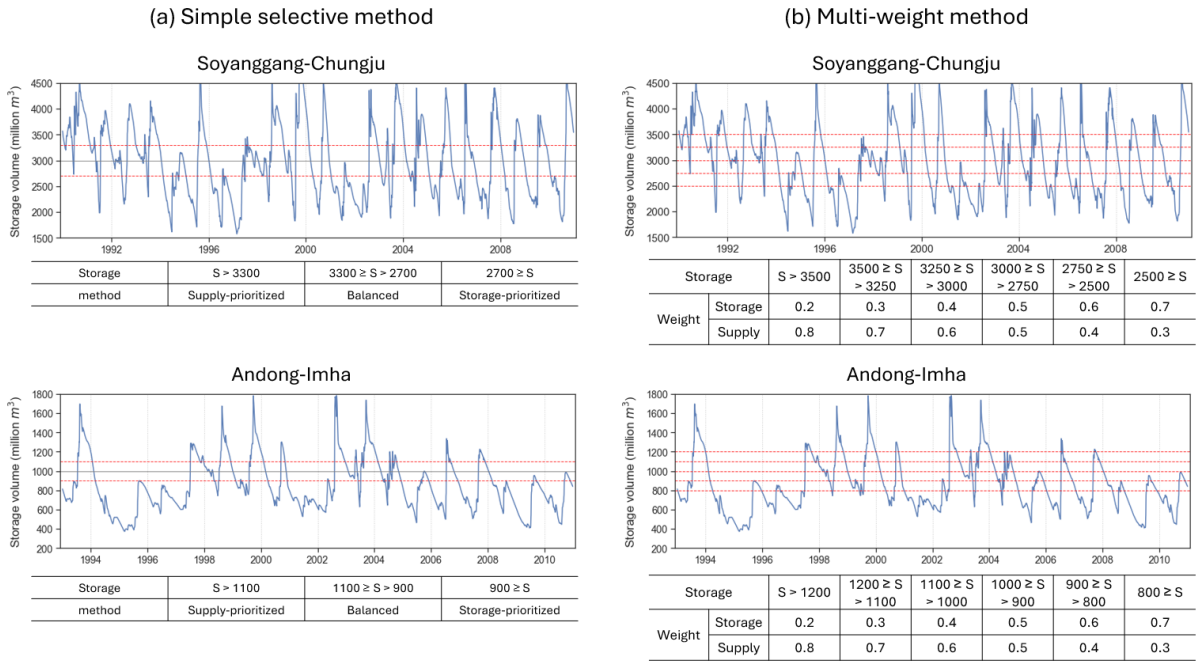

Figure SI: (a) Simple selective method: the storage ranges and applied SAW method in each range. (b) Multi-weight method: the storage ranges and applied weight in each range. The blue lines represent the daily reservoir operation records for Soyanggang-Chungju (first row) and Andong-Imha (second row) reservoir systems.

The reference point method identifies the compromise solution on a Pareto front by measuring the distance from a reference point. In this study, we applied three versions of this approach: 'utopian point', 'knee point', and 'TOPSIS' methods. Application examples of these methods are illustrated in Figure SII.

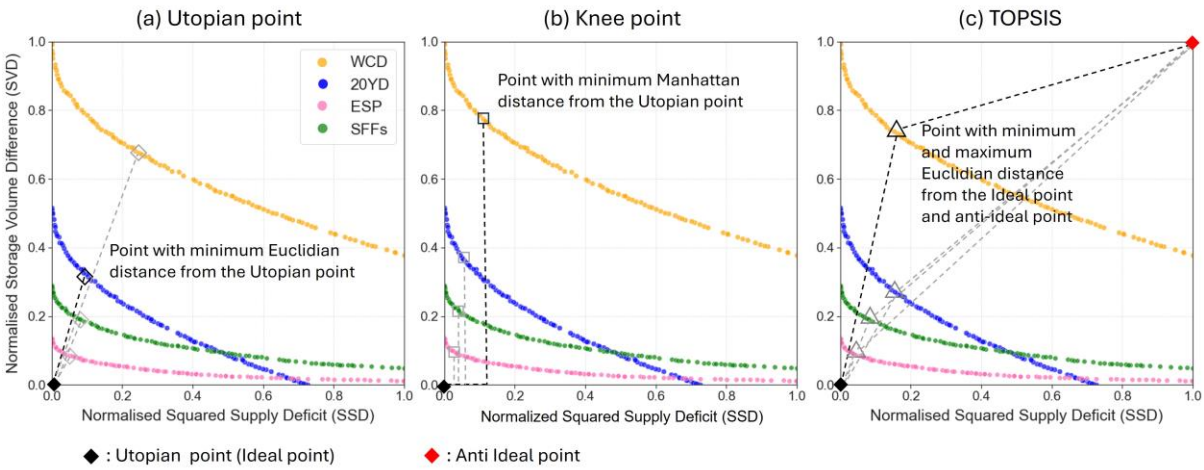

Figure SII: An example of the reference point method, including (a) Utopian Point, (b) Knee Point, and (c) TOPSIS method, generated for June 2014 with a 4-month lead time using different flow forecasts (WCD: yellow, 20YD: blue, ESP: pink, SFFs: green).

The utopian point method selects the solution on the Pareto front that minimizes the Euclidean distance from the utopian (or ideal) point, which represents the theoretical perfect solution (Lu et al., 2011). The knee point method selects the knee point, which is a point where the curvature of the Pareto front is maximum (Das, 1999). Among various methods for detecting the knee point, we adopted the approach based on Minimum Manhattan Distance from the utopian point (Chiu et al., 2016). This approach has been demonstrated to be both simple and robust in the literature (Li et al., 2020). Compromise solutions from these two methods are computed as:

$$Compromise\ solution_{Utopian} = \min\left(\sqrt{\left(SSD_i - SSD_{utopian}\right)^2 + \left(SVD_i - SVD_{utopian}\right)^2}\right) \quad \text{(S3)}$$

$$Compromise\ solution_{Knee} = \min(|SSD_i - SSD_{utopian}| + |SVD_i - SVD_{utopian}|) \quad \text{(S4)}$$

where $i = 1, \ldots, 100$ is the number of points (each corresponding to a Pareto-optimal release schedule) on the Pareto front. SSD_i and SVD_i denote a normalized point of each objective at the ith point (see Eqs. 5 and 6 in main manuscript). SSD_{utopia} and SVD_{utopia} are the utopian points of each objective, which are equal to [0, 0].

The TOPSIS method, developed by Hwang and Yoon (1981), is a widely chosen method for MCDM (Tzeng and Huang, 2011; Wang and Rangaiah, 2017) and is recommended by the United Nations Environmental Program (Chen, 2000; Zhu et al., 2015). It selects a point with the shortest Euclidian distance from the ideal point [0, 0] and the longest distance from the anti-ideal point [1, 1] as the compromise solution (Hwang and Yoon, 1981; Liu, 2009). This can be expressed as:

$$Distance_i^{ideal} = \sqrt{(SSD_i - SSD_{ideal})^2 + (SVD_i - SVD_{ideal})^2} \quad \text{(S5)}$$

$$Distance_i^{anti-ideal} = \sqrt{(SSD_{anti-ideal} - SSD_i)^2 + (SVD_{anti-ideal} - SVD_i)^2} \quad \text{(S6)}$$

$$CC_i = \frac{Distance_i^{anti-ideal}}{Distance_i^{ideal} + Distance_i^{anti-ideal}} \quad \text{(S7)}$$

where $Distance_i^{ideal}$ and $Distance_i^{anti-ideal}$ are the Euclidian distances from ideal and anti-ideal points from ith point, and CC_i is the closeness coefficient of the ith point. Since a higher closeness coefficient indicates a better solution, the point with the highest CC_i is selected as the compromise solution.

S3. Supplementary figures

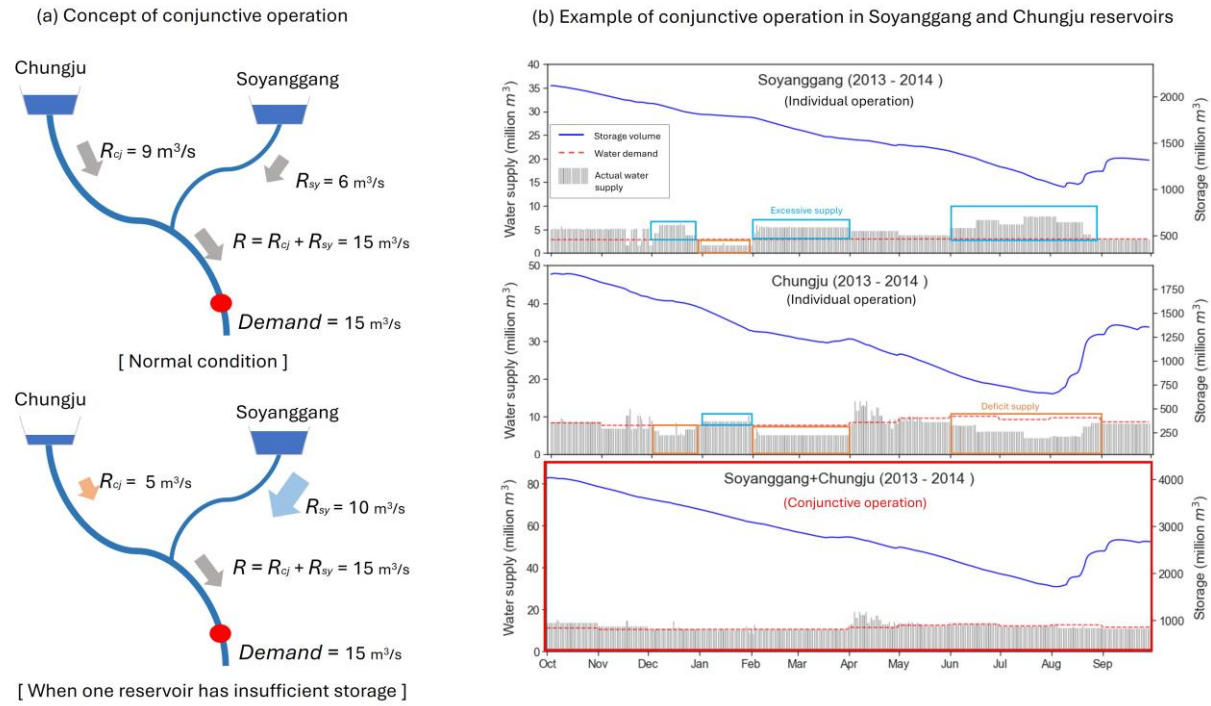

Figure S1: (a) Concept of conjunctive reservoir operations. (b) Daily reservoir operation records from October 2013 to September 2014 for Soyangang reservoir alone (first row), Chungju reservoir alone (second row) and their conjunctive operation (third row).

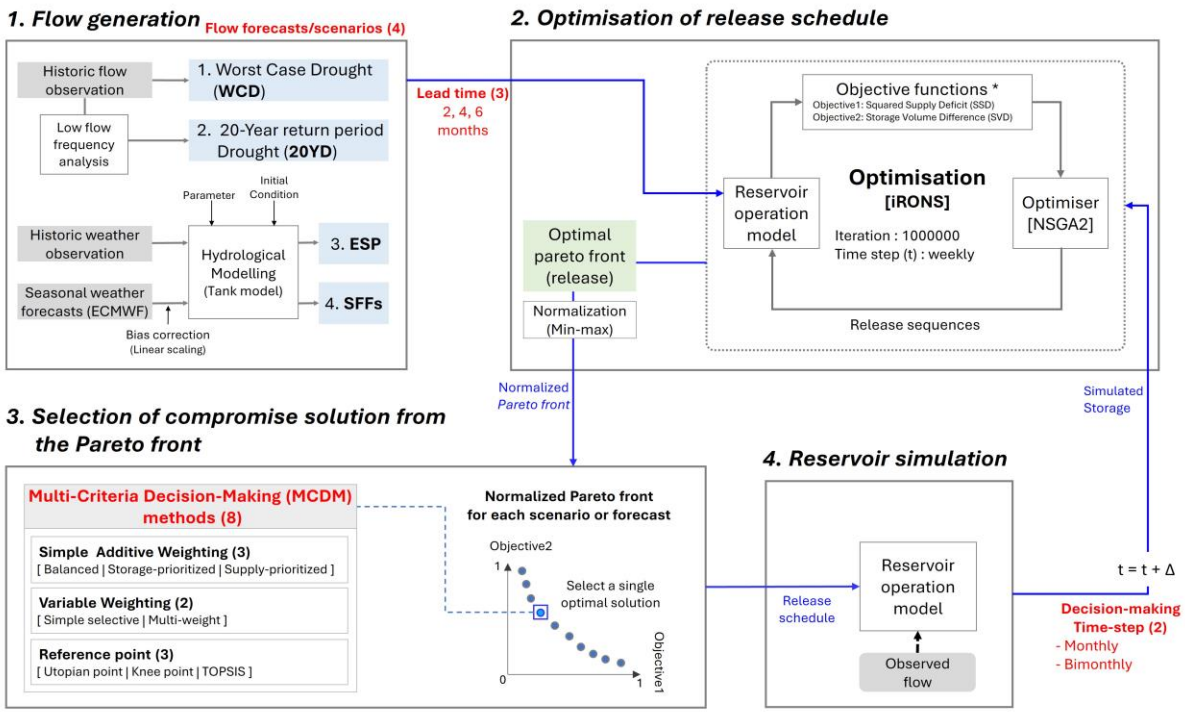

* **Objectives**: minimizing **mean Squared Supply Deficit** (**SSD**) and **Storage Volume Difference** (**SVD**) at the end of wet season.

Figure S2: Sophisticated schematic diagram depicting the reservoir simulation method employed in the study.

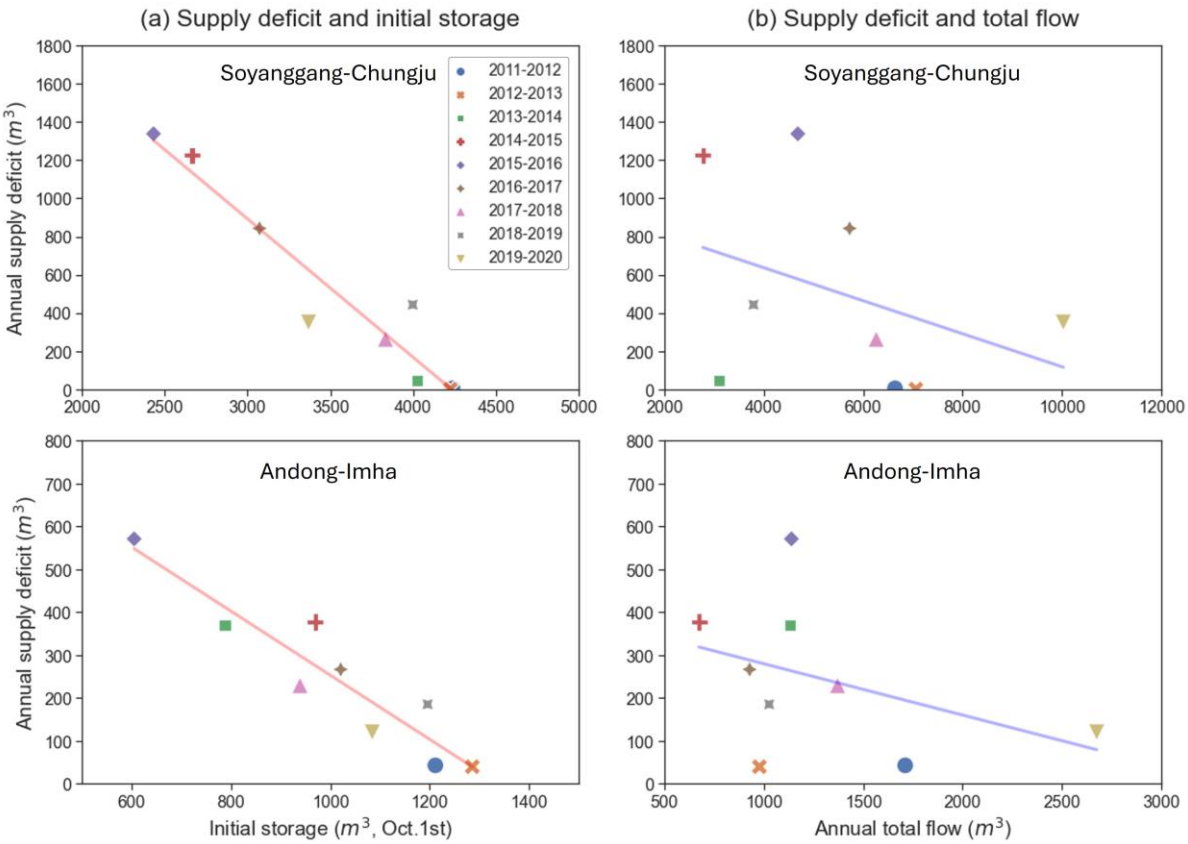

Figure S3: Historical relationship between annual supply deficit (y-axis) and (a) initial storage at the beginning of new hydrological year (October 1st) or (b) annual total flow into reservoir over a hydrological year from 2011 to 2020. Frist and second rows represent Soyanggang-Chungju and Andong-imha reservoir systems, respectively.

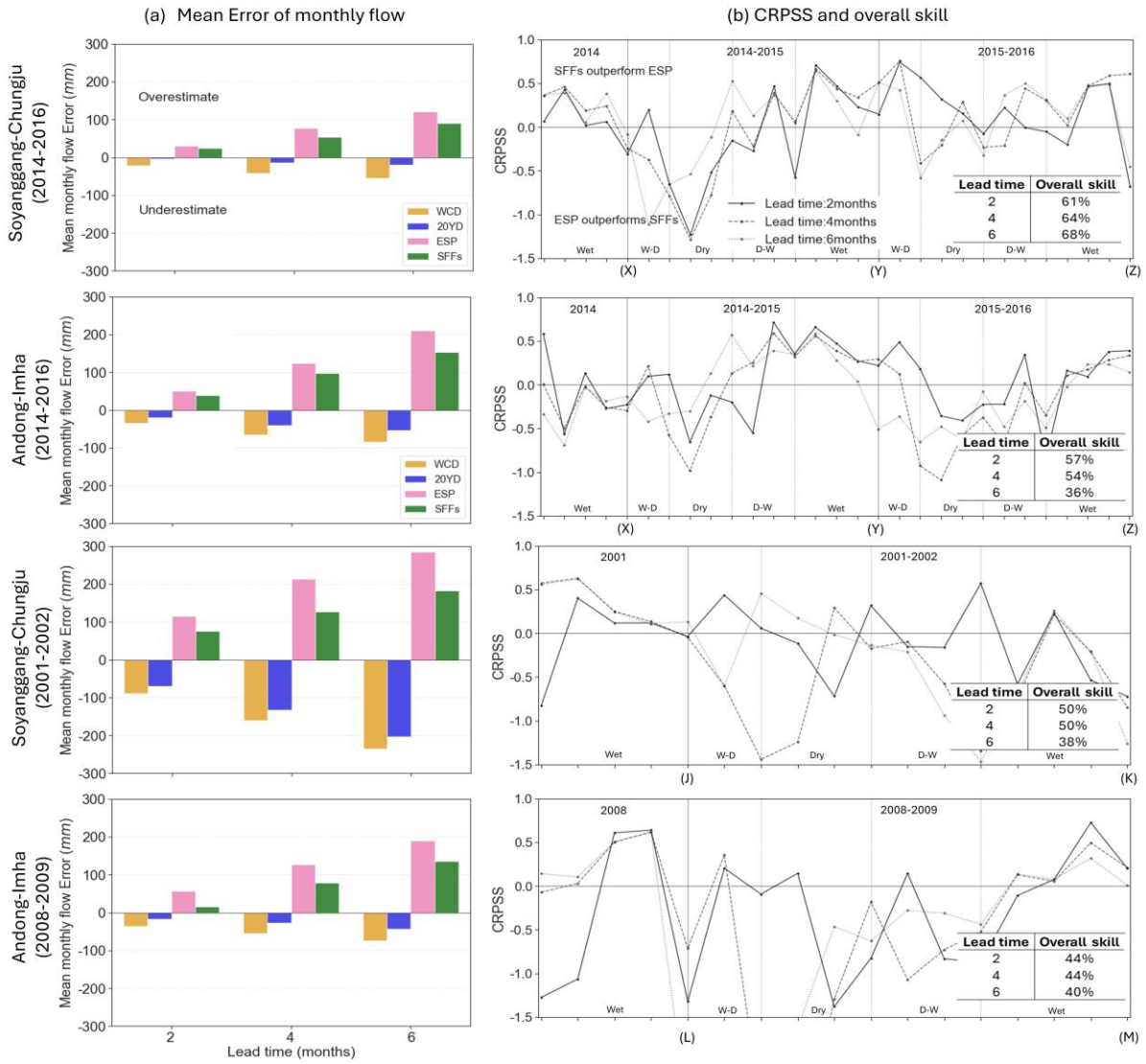

Figure S4: (a) Mean Error of monthly flow (optimised – observed) for 2-month lead time. (b) CRPSS at lead time 2, 4 and 6 months (line plot) and overall skill which represents the frequency of SFFs outperforming ESP (table, bottom right). From top to bottom, the rows represent Soyanggang-Chungju for 2014-2016, Andong-Imha for 2014-2016, Soyanggang-Chungju for 2001-2002 and Andong-Imha for 2008-2009.

1. Andong-Imha (2014-2016)

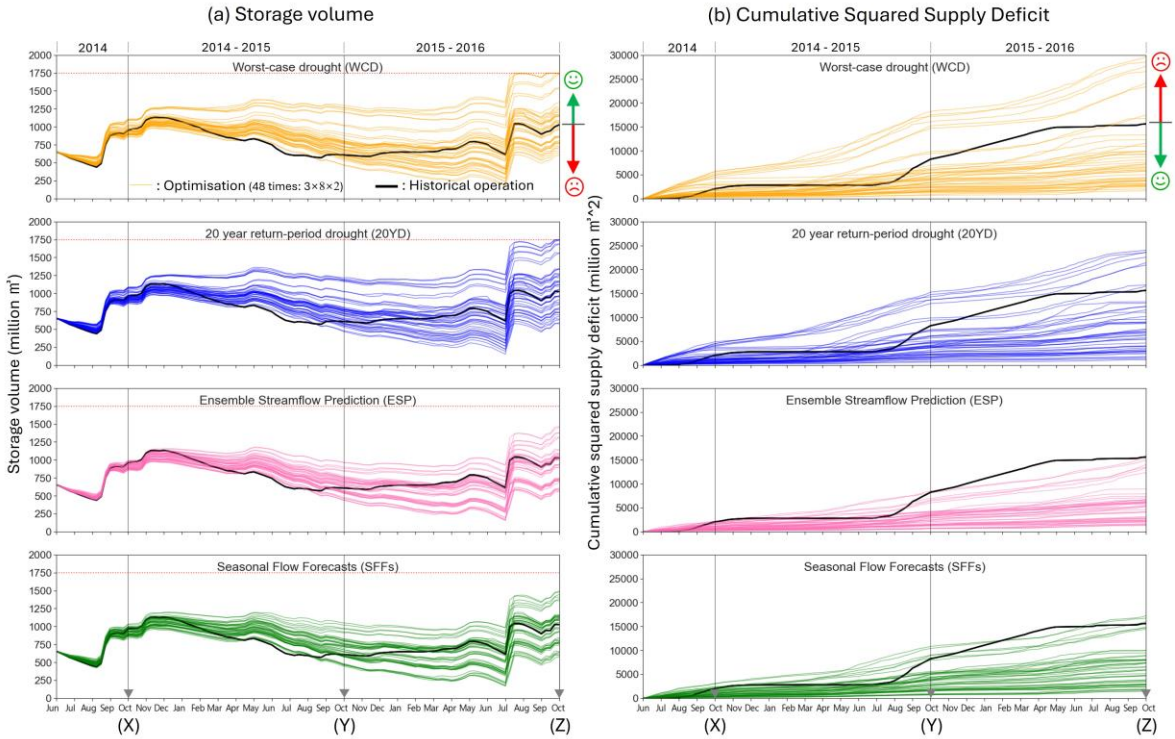

2. Soyanggang-Chungju (2001-2002)

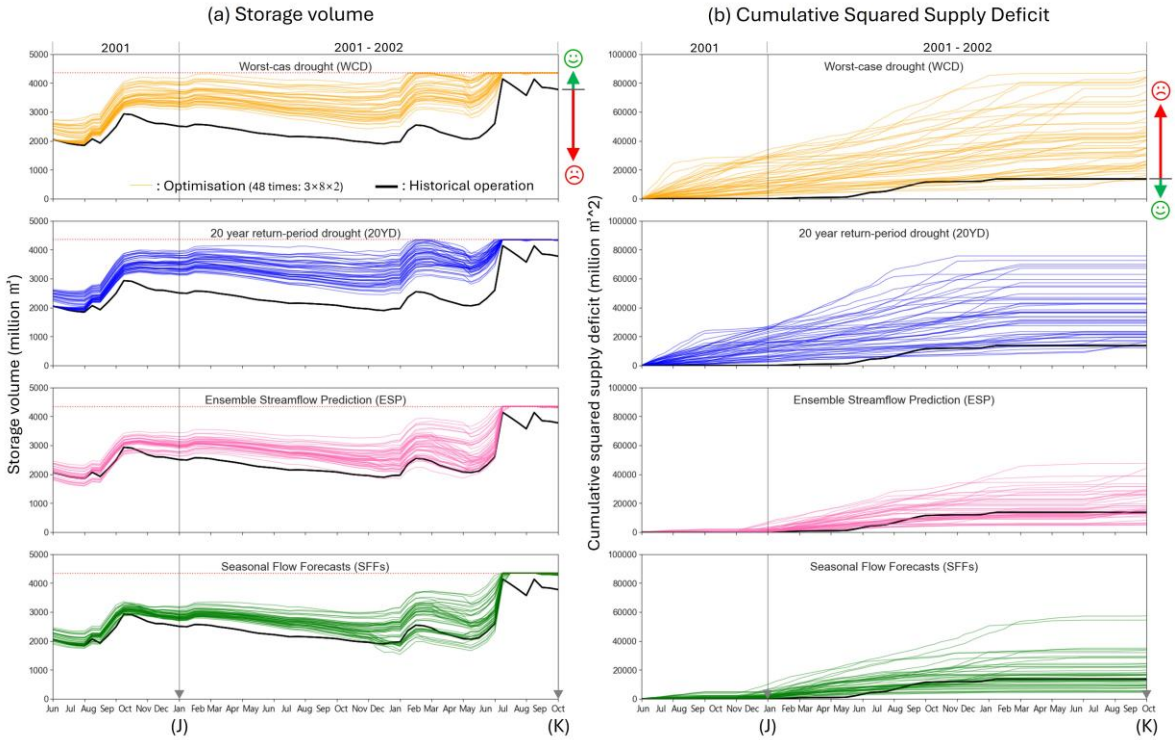

3. Andong-Imha (2008-2009)

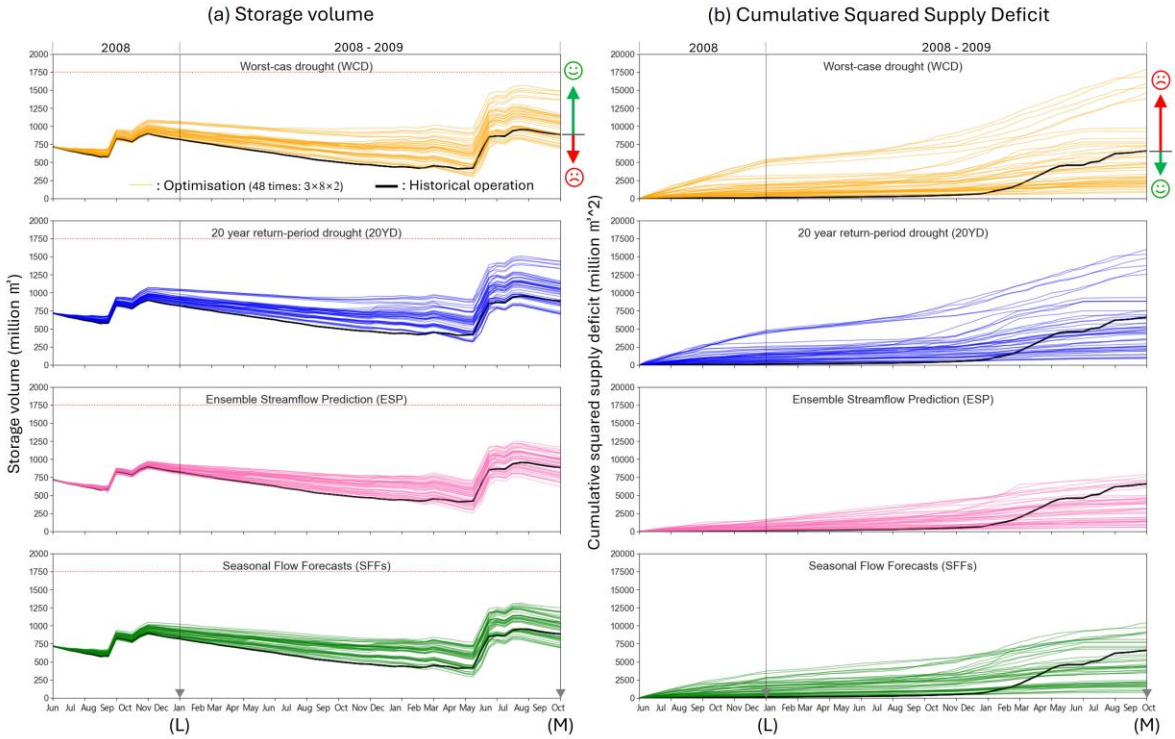

Figure S5: Simulated reservoir operation results for (1) Andong-Imha from June 2014 to September 2016, (2) Soyanggang-Chungju from June 2001 to September 2002 and (3) Andong-Imha from June 2008 to September 2009, in terms of (a) are storage volume and (b) cumulative squared supply deficit. From top to bottom, the rows represent simulation results generated by using WCD (orange), 20YD (blue), ESP (pink), and SFFs (green), respectively. Each sub-figure has 48 simulated results (coloured lines, 3 lead times × 8 MCDM methods × 2 decision-making time steps) and a single historical operation (black line).

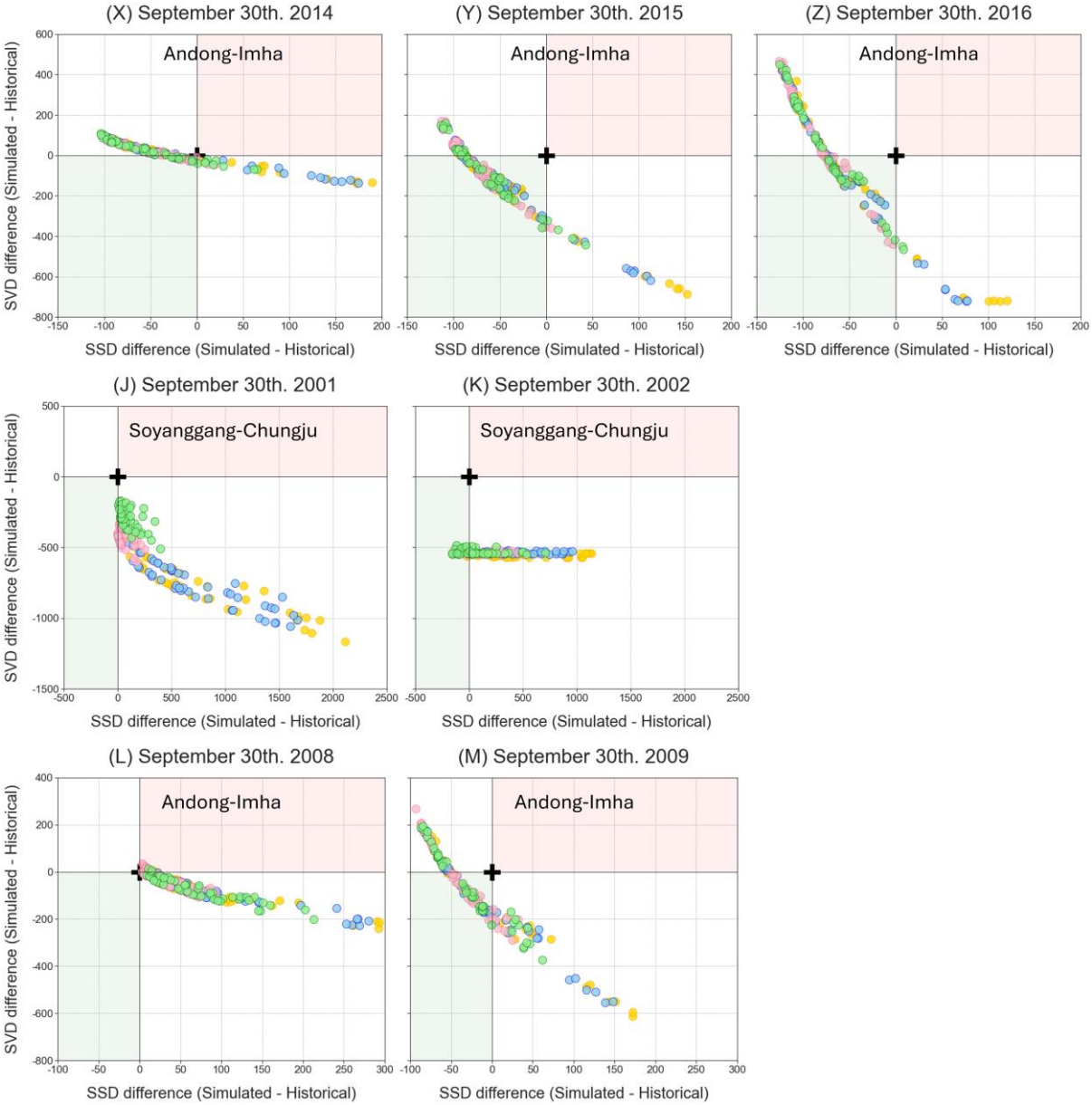

Figure S6: Difference of SSD (x-axis) and SVD (y-axis) between historical operation (black cross) and simulate operations using different flow forecasts/scenarios (coloured circles) in (first row) Andong-Imha during 2014-2016 drought, (second row) Soyanggang-Chungju during 2002-2003 drought and (third row) Andong-Imha during 2008-2009 drought, respectively. Performances are calculated on September 30th in (first row) 2014 (X), 2015 (Y), 2016 (Z) and (second row) 2001 (J), 2002 (K) and (third row) 2008 (L), 2009 (M). Each sub-figure shows 48 points for each flow forecast/scenario (WCD, 20YD, ESP, SFFs), resulting from different combinations of key experimental choices (3 lead times × 8 MCDM methods × 2 decision-making time steps).

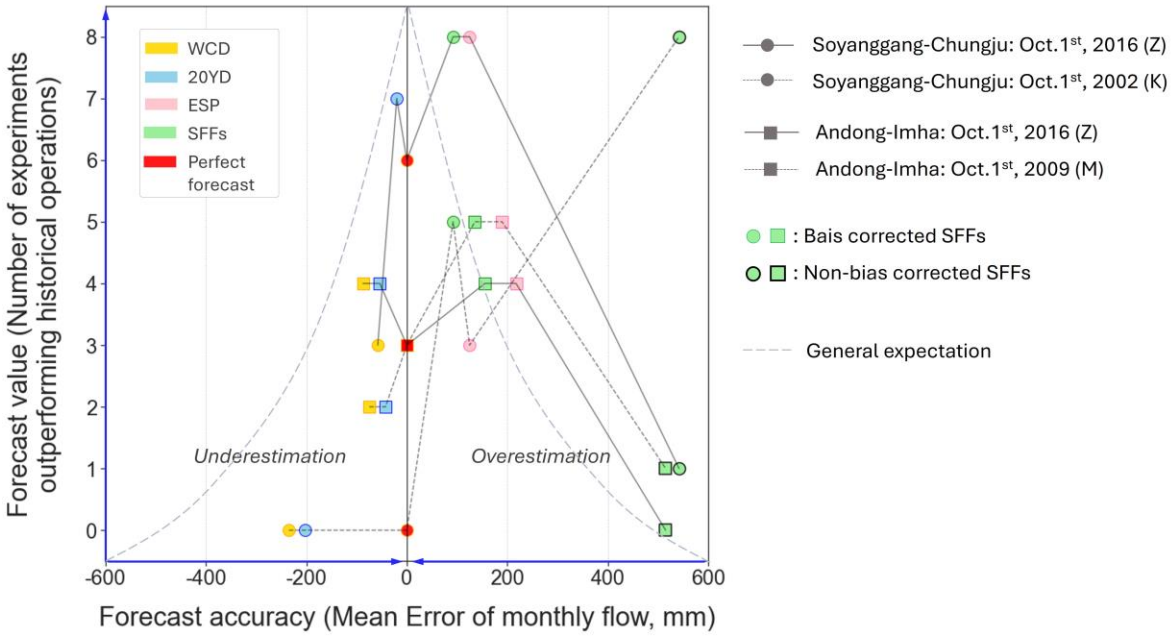

Figure S7: Relationship between forecast accuracy (mean error of monthly flow, mm) and value at the end of the simulation period for different drought events (2002, 2009 and 2016) at Soyanggang-Chungju and Andong-Imha reservoir systems. For each event and system, the figure shows five points corresponding to simulated forecast-informed operations using different forecast/scenarios (orange: WCD, blue: 20YD, pink: ESP, green: SFFs, red: perfect forecast). Here, green symbols with (without) outlines represents bias corrected (non-bias corrected) SFFs, respectively. The direction of the blue arrows indicates higher performance (high value, low error). The grey dashed lines represent the general expectation on the relationship between forecast accuracy and value.